https://doi.org/10.15407/ufm.27.03.542

M.O. VASYLYEV [1,*], B.M. MORDYUK [1,], S.M. VOLOSHKO [2,***], and P.O. HURYN [3,****]**

[1] G.V. Kurdyumov Institute for Metal Physics of the N.A.S. of Ukraine, 36 Academician Vernadsky Blvd., UA-03142 Kyiv, Ukraine

[2] National Technical University of Ukraine 'Igor Sikorsky Kyiv Polytechnic Institute', 37 Beresteiskyi Ave., UA-03056 Kyiv, Ukraine

[3] P.L. Shupyk National Healthcare University of Ukraine, 9, Dorogozhytska Str., UA-04112 Kyiv, Ukraine

*vasil@imp.kiev.ua, ** mordyuk@imp.kiev.ua,
*** voloshkosvetlana13@gmail.com, **** dr.huryn17@gmail.com

FRACTURE SURFACE ANALYSIS OF THE FATIGUE-FAILED TITANIUM DENTAL IMPLANTS

In recent years, the osseointegrated titanium dental implants have revolutionised the field of dentistry owing to their ability to restore oral function. Thus, they have been widely used for decades with high survival and success rates. Such prosthetic devices demonstrate high long-term success rates. However, mechanical complications similar to fatigue fracture remain the clinically significant cause of late implant failure. It is one of the important biomechanical complications that can present a considerable problem to the patient and the dentist. This article aims to elucidate the microstructural mechanism of fatigue failure of titanium dental implants. The fracture surfaces of two types of failed implant samples made of technically (commercially) pure titanium (c.p. Ti) and the Ti–6Al–4V alloy are studied. The specimens of the first type are tested in laboratory conditions under the action of cyclic loading in accordance with the European normative used for the mechanical tests (UNI EN ISO 14801); the other implant specimens are taken from the patient after their failure. The use of scanning electron microscopy (SEM) on the fracture surface provides information about the failure-initiation site, loading history, environmental effects and surface-material quality of the

Citation: M.O. Vasylyev, B.M. Mordyuk, S.M. Voloshko, and P.O. Huryn, Fracture Surface Analysis of the Fatigue-Failed Titanium Dental Implants, *Progress in Physics of Metals*, **27**, No. 3: 544–567 (2026)

implant body and abutment. SEM allowed confirmation that fatigue is the main implant-failure mechanism comprising a three-stage pathway well-known for metals, *i.e.*, a stable crack propagation followed by accelerated crack propagation with apparent striations, and a final fast failure by voids' nucleation, coalescence, and growth. Despite compliance with the requirements for the implant microstructure, stress concentration on the implant constructive peculiarities and corrosion damage, which can be induced by the aggressive oral environment, increases the fatigue-failure risk.

Keywords: dental implants, titanium, Ti–6Al–4V alloy, fatigue failure, cyclic loading, implant fracture.

1. Introduction

For many years, dental implants have emerged as a successful and widely used treatment option in modern dentistry, providing both functional and aesthetic solutions to patients with partially or edentulous jaws for replacing missing teeth. In recent years, with their ability to restore oral function, dental implants have revolutionised the field of dentistry [1–4]. Most dental implants are manufactured as a two-piece system, which consists of two functional components: the fixture (body) and the abutment (Fig. 1). The fixture is the endosteal component, which is placed in the bone volume during the first surgical procedure. The abutment is the adapter head that is screwed to the implant body after implant osseointegration, and on which the crown (or any other prosthetic design) is fixed on the fixture top to support the prosthetic restoration [5, 6].

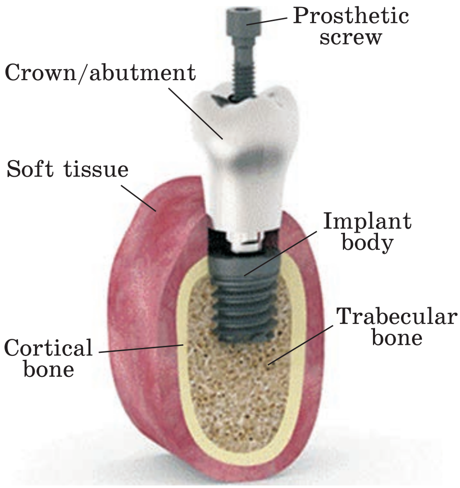

Fig. 1. Assembly of the single dental implant restoration [7]

Clinical practice has established that the success of the implant treatment depends on a variety of factors that are specific to the implant itself (*e.g.*, design, material, and surgical procedure), the patient, or the actual method used to place the implant.

2. Mechanical Complications and Implant Failures

The major concern for the dentist and patient is the durability of the dental implant. Factors such as implant design, surface properties, and the manufacturing surgical process can influence the success rate of the implants. Recent research also found that the oral environment and the actual implantation procedure may have related to the success of the implants as important as the above-mentioned factors. Many longitudinal studies have reported osseointegrated dental implant success and survival rates of close to 90–95% [8–10]. However, despite their overall success, failures and complications associated with dental implants can occur, with fractures and mechanical failures being significant concerns. Dental implant failures can be classified into two categories: biological and mechanical. Biological failures primarily involve issues related to osseointegration, peri-implantitis (inflammation and bone loss around the implant), and soft tissue complications.

On the other hand, mechanical failures encompass fractures and other structural problems directly associated with the implant components. These failures can take place in the abutment, in the implant body or in the prosthetic screw, depending on implant diameter, load case, implant position, *etc*. Nevertheless, screw failures are the most common as compared to failures of the abutment or implant [11–16].

Implant fracture is a major cause of late prosthetic implant failure, as one of the possible complications of the implant. The incidence of implant body fracture reported is 0.98–1.5% [17]. It was found that mechanical complications included abutment and prosthesis screw loosening, abutment and prosthesis screw fractures and implant fractures. The incidence of abutment screw loosening was reported to be between 2 and 45%, depending on the type of prosthesis, and abutment screw fracture occurs less frequently, with an incidence of 0.5–8%. Prosthesis screw loosening ranged from 1 to 38%, and their fracture rate ranged from 1 to 19%. Fortunately, the incidence of implant fracture is far less, reported to be 0.2–3.5% [18]. Several reasons can increase the incidence and cause of titanium implant fractures. According to a literature review, they can be summarised as poor implant manufacturing or implant design and defects, implant–abutment misfit, unfavourable occlusal loading with biomechanical or physiologic overloading, bone resorption, loss of supporting tissue secondary to infection or peri-implantitis, implant diameter, and galvanic implant corrosion [19–24].

The design of the implantable dental implants must always take into consideration the cyclic loads the implant will undergo throughout its lifetime. The fatigue endurance of the materials used will play a very important role when trying to estimate the long-term performance of the device. Thus, the assessment of the fatigue behaviour of the implantable alloys has acquired greater importance. Metal fatigue due to biomechanical overloading appears to be the most frequent cause. The fatigue life of the implant depends on both the implant itself and the physical properties of the bone, as well as on other morphological characteristics that are patient-dependent, which explains why this fatigue life varies greatly with each newly placed implant [25–27].

Titanium and its alloys are appreciated as the implant materials in dentistry since the discovery of osseointegration by Brånemark [28, 29].

Commercially pure titanium (c.p. Ti) is one of the most often used materials for oral implants owing to its biocompatibility, moderate strength, fatigue and corrosion resistance, as well as the low specific weight [30–34].

3. Laboratory Fatigue Tests

The laboratory fatigue testing setup for the dental implants is designed to apply cyclic loading under controlled conditions in accordance with the European normative used for the mechanical tests (UNI EN ISO 14801). Such a testing system simulates worst-case clinical loading of the endosseous dental implant, providing a reliable framework for reproducing fracture mechanisms observed in failed dental implants. The scheme and view of the positioning system, which is applied for the complete tests and implants without an angled connection, are shown in Fig. 2 and Fig. 3. In particular, the sample was placed at 30° relative to the implant's longitudinal axis [37–41]. After the fractographic examination of the fatigue-tested implants, identification of the crack initiation sites, crack propagation behaviour, and the final fracture modes contributes to improved implant design and enhanced long-term clinical reliability.

Loading conditions during the fatigue testing are as follows: sinusoidal cyclic load ratio (R = 0.1), frequency of 2–15 Hz, number of 2–5 million cycles, environment air or saline solution (optional). Stress (S) versus number of cycles to failure (N), used to compare implant designs and materials (S–N curves). Cyclic loading is applied using a servo-hydraulic or electrodynamic testing machine. The importance of fatigue testing, which predicts long-term clinical reliability, allows comparison between implant systems and identifies weak points in design. The fatigue testing of dental implants is

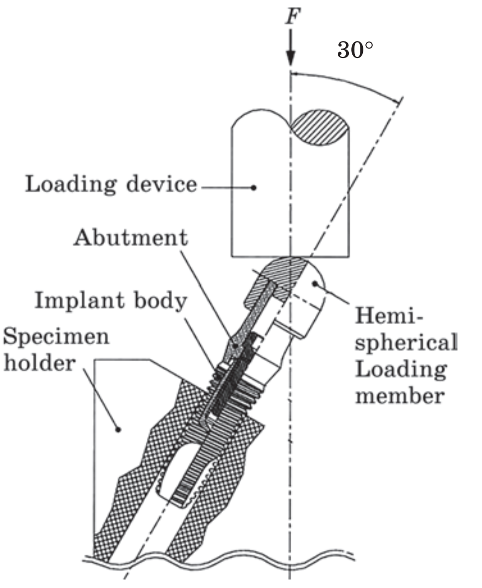

Fig. 2. Schematic diagram of the fatigue testing [35]

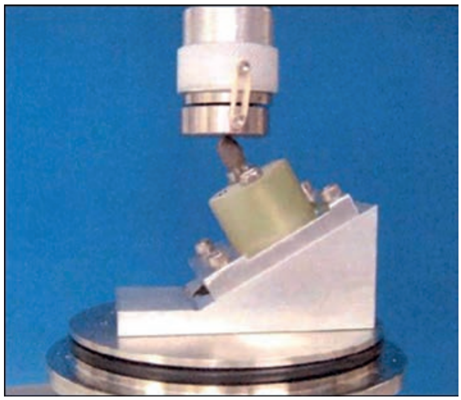

Fig. 3. Schematic set-up according to the ISO 14801 protocol [36]

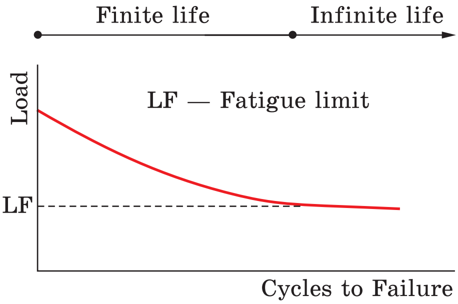

Fig. 4. The sample S–N curve for titanium [36]

the key experimental method for investigating the fracture mechanisms leading to implant fractures. Engineering fatigue data is most commonly presented in the form of an S–N curve, where stress (S) is plotted against the number of cycles to failure (N). This data is useful for lifetime prediction analysis. Generally, as the stress decreases, the metal endures a greater number of cycles; below a certain stress, the S–N curve levels off and becomes horizontal at the particular stress level. This stress level is known as the fatigue limit. Below this limit, the metals can theoretically endure an infinite number of cycles without failure (Fig. 4). The S–N curve is generated by testing multiple specimens at varying loads and recording the number of cycles to failure. Traditionally, this has required a larger number of specimens due to the wide distribution of both failure loads at a constant number of cycles and the number of cycles to failure at a constant load. Generating this data would be difficult due to the high costs of the implants and the time required for testing dozens of specimens for millions of cycles.

4. Implant Body Failure

Evaluation of the body titanium dental implant fracture surface after fatigue testing using SEM was performed in Ref. [42]. The fatigue testing in dry conditions was carried out with sinusoidal and unidirectional load (Standardized parameters according to UNI EN ISO 14801). The testing was performed in the air (20±5°C) at frequencies up to 30 Hz until failure or five million cycles. Using the higher-magnification SEM images, it was revealed that the three distinct stages of the body failure surface crack evaluation, specifically the crack pop-in and arrest, the fatigue crack growth and the catastrophic or ductile failure. Figure 5 shows the SEM image series for the failed body implant. It can be noted that these three stages of the crack growth contain representative topographical differences. In particular, region A represents the crack pop-in phase, region B represents fatigue crack growth, and region C represents the ductile failure region.

These three zones are normally observed in the fracture surfaces of various metallic materials experiencing fatigue induced by cyclic loading [43–46], including pure titanium [47–49] and Ti–6Al–4V alloy [49, 50]. Precisely, the crack initiation area with adjoined zone ‘A’ of stable crack propagation is followed by zone ‘B’ of accelerated crack propagation with apparent striations, and a final fast fracture zone ‘C’, which exhibits fai-

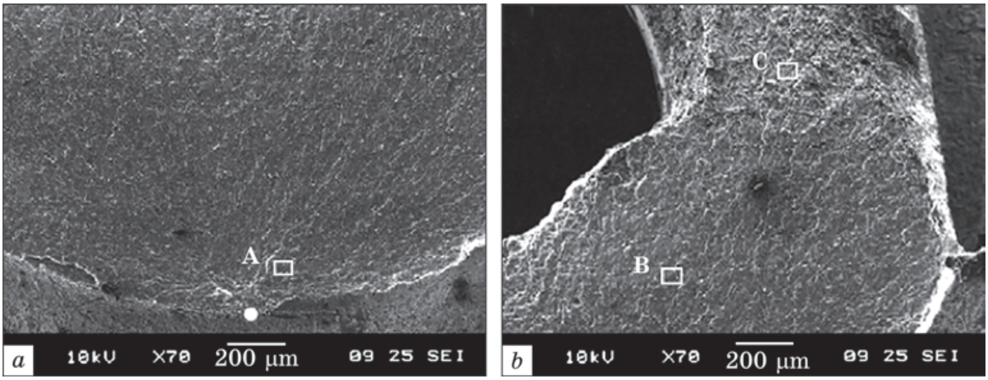

Fig. 5. SEM images of three zones of the crack growth: *a* — stable crack propagation (*A*), *b* — accelerated crack propagation (*B*) and failure by void nucleation (*C*); the dot in the left figure (*a*) indicates the crack origin [42]

lure by void nucleation, coalescence and growth. Two different stages, *viz.*, the stage prior to short crack initiation in high-cycle fatigue (HCF) and the stage of long crack propagation in low-cycle fatigue (LCF), are known to be identified in fatigue behaviour of metallic materials [44, 51]. In the HCF regime, low applied stress amplitudes are known to be well below the tensile and compressive yield stress, and they induce predominantly elastic strains in the material during the test, with most of the fatigue life spent on crack initiation in this regime. Thus, the higher the strength of the material is, the better the resistance against crack nucleation. On the contrary, plastic strain amplitudes are dominant in the LCF regime as the applied stress amplitudes exceed the yield stress considerably. Therefore, the ductility of the material becomes determinative in the fatigue damage tolerance in this case.

The fracture surface within the crack pop-in region (zone '*A*' of stable crack propagation) at high magnification is presented in Fig. 6, *a*. As one can see, such a fracture surface is relatively smooth and represents transgranular crack growth with little or no grain boundary involvement, and no fatigue striations are evident. The stage II crack growth (zone '*B*') exhibits crack-arrest marks known as the fatigue striations (an example of which is shown in Fig. 6, *b*), which are the result of one load cycle. It is expected that the general direction of the crack propagation is from the bottom of the image to the top, and the majority of the fatigue striations are aligned perpendicular to this. In addition, one can see that the microcracks between the grains and within some of the grains, the fatigue striations follow a different direction than expected. Furthermore, the crack is progressing on multiple plateaus at different elevations. A ductile failure region (a final fast fracture zone '*C*') occurred when the fractured implant was manually detached. Figure 6, *c* shows the characteristic image of this fracture mode. Evidently, the cup-like depressions are also

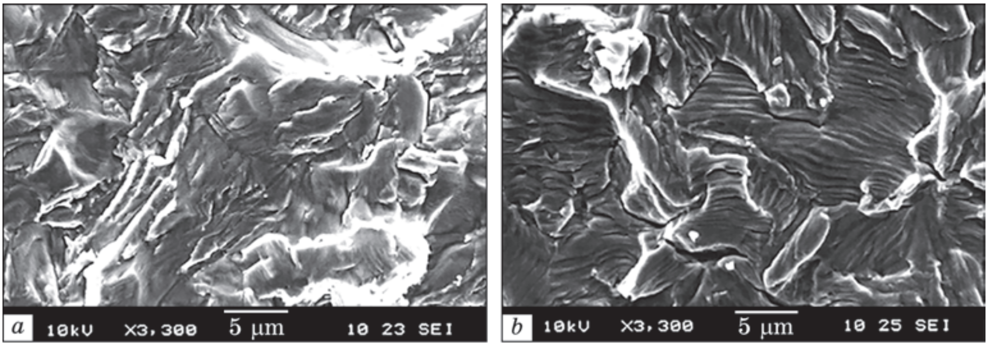

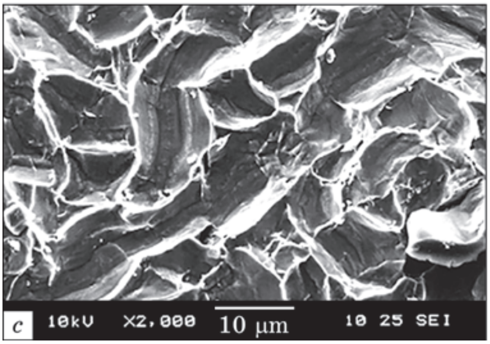

Fig. 6. The SEM images at high magnifications: *a* — the crack pop-in stage of the failure corresponding to the location *A* shown in Fig. 5; *b* — the representative fatigue crack growth corresponding to location *B* in the previous figure; *c* — the ductile failure corresponding to the location *C* in Fig. 5 [42]

known as dimples. As the strain was applied, the microvoids in the alloy grew and coalesced. The lip or rim of the dimples is the result of the fracture surfaces final separation. In addition, the dimples are non-uniformly shaped, with some being round and others being more elongated.

It was demonstrated that the majority of the implants failed at less than 250 000 cycles. The fatigue life of 125 000 cycles is the mean failure period for this group. The fatigue striations would align perpendicularly to the overall direction of the crack propagation.

The effect of commercial dental implant diameter on load fatigue testing in air and in a simulated oral environment was studied in [52]. Three types of implants were tested with an outer diameter of 3.3 mm, 3.75 mm, and 5 mm. To minimise vibration of the instrument during testing fatigue life according to UNI EN ISO 14801, the applied cyclic load had a sinusoidal force with a frequency of 15 Hz in air at a temperature of $20 \pm 5°$. In the simulated physiological environment, the fatigue testing was conducted at a frequency of 2 Hz. Normal saline with 0.9% NaCl, as an artificial body fluid to simulate the implant being immersed in blood and saliva, was used in this study. From the S–N curve results (in air) for the three implant diameters, significant differences were observed. In particular, for the 3.75-mm diameter implant, the normalised load decreased as the mean number of cycles to failure increased, and the probability of survival increased as the normalised load decreased. For the 5-mm diameter

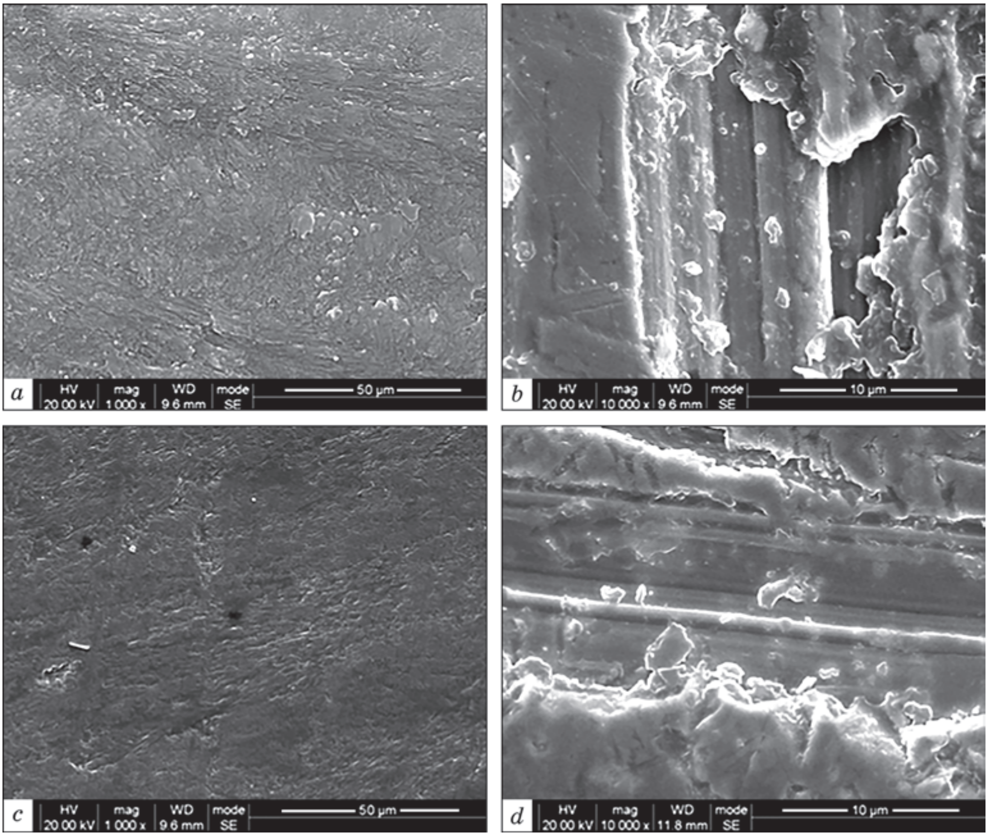

Fig. 7. (*a*) The implant surface fractured in the simulated body with the low magnification. (*b*) The fractured implant surface in the air with the low magnification. (*c*) The fracture surface of the implant fractured in the simulated body environment with the high magnification. (*d*) The fracture surface of the implant fractured in the air with high magnification [52]

implant, the normalised load decreased as the average number of cycles to failure increased. In contrast, the 3.3-mm-diameter implant, which had a different probability of survival from the other two implants, did not increase monotonically as the normalised load decreased. The fatigue limit of all of the implants tested in the simulated oral environment was lowered by 20% compared to that under air conditions. It was pointed out that the simulated oral physiological environment influenced the fatigue strength by producing a corrosive environment that affected the fatigue mechanism. The typical microphotographs of the fracture surfaces in two kinds of conditions are shown in Fig. 7. It can be seen that the implant surfaces were broken at a similar load level. However, the fatigue striations in the simulated body showed transgranular fracture with secondary cracking, which was not found in the air testing instead.

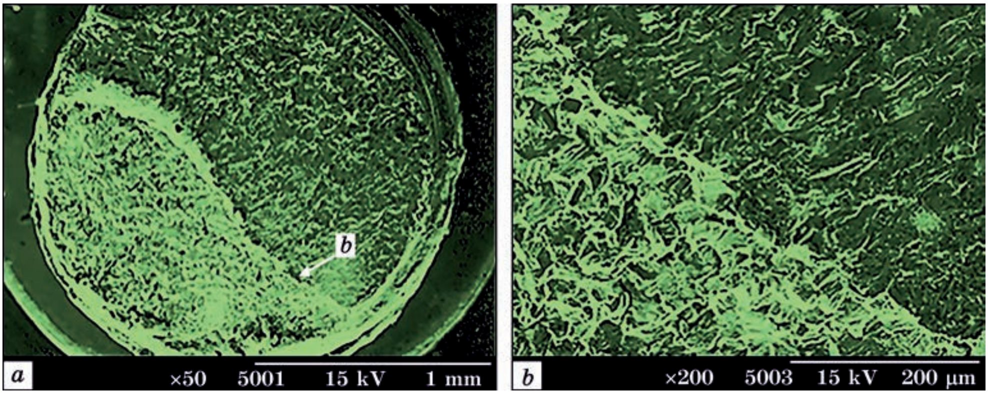

Fig. 8. Typical scanning electron photomicrographs from the fracture surface of the failed abutment screw [53]

5. The Implant Abutment Fatigue Fracture

The fracture surface analysis of the pure titanium implant abutment was tested in the study [53]. The system consisted of the 10-mm implant with an outer diameter of 3.75 mm, the cylindrical abutment with a height of 8 mm, and the abutment screw to connect the components. To produce fatigue-fracture samples, the cyclic load was applied to the implant according to the protocol UNI EN ISO 14801. The applied cyclic load was set as a sinusoidal force with a frequency of 15 Hz. The test machine was set to automatically shut off when the specimen failed or the cyclic loading reached $5\cdot10^6$ cycles. The fatigue-fracture surface of the fractured implant components was examined using SEM. In this study, the smooth region ratio (SRR) was defined as the ratio of the smooth phase area to the area of the whole fracture surface. The typical SEM images of the fractured abutment screw are exhibited in Fig. 8. As seen, the smooth and rough surfaces at the tension and compression sites are formed, respectively. The significant boundary between the smooth and rough regions can be seen on the fracture surface. In addition, the crack propagation direction can be identified from the lines parallel to the dimpled lines in the smooth region. The fatigue fracture has been explained as the propagation of microscopic cracks caused by the stress concentration in the structural analysis.

6. The Fracture Surface of the Retrieved Failed Implants

When the titanium implant fracture surfaces are examined using SEM, the first observed feature is the macroscopically different contrast between the stable fatigue crack growth region, followed by the catastrophic overload (Fig. 9, *a*) [54]. In the fatigue region, the characteristic feature of fine parallel lines (striations) can be discerned to a variable extent at

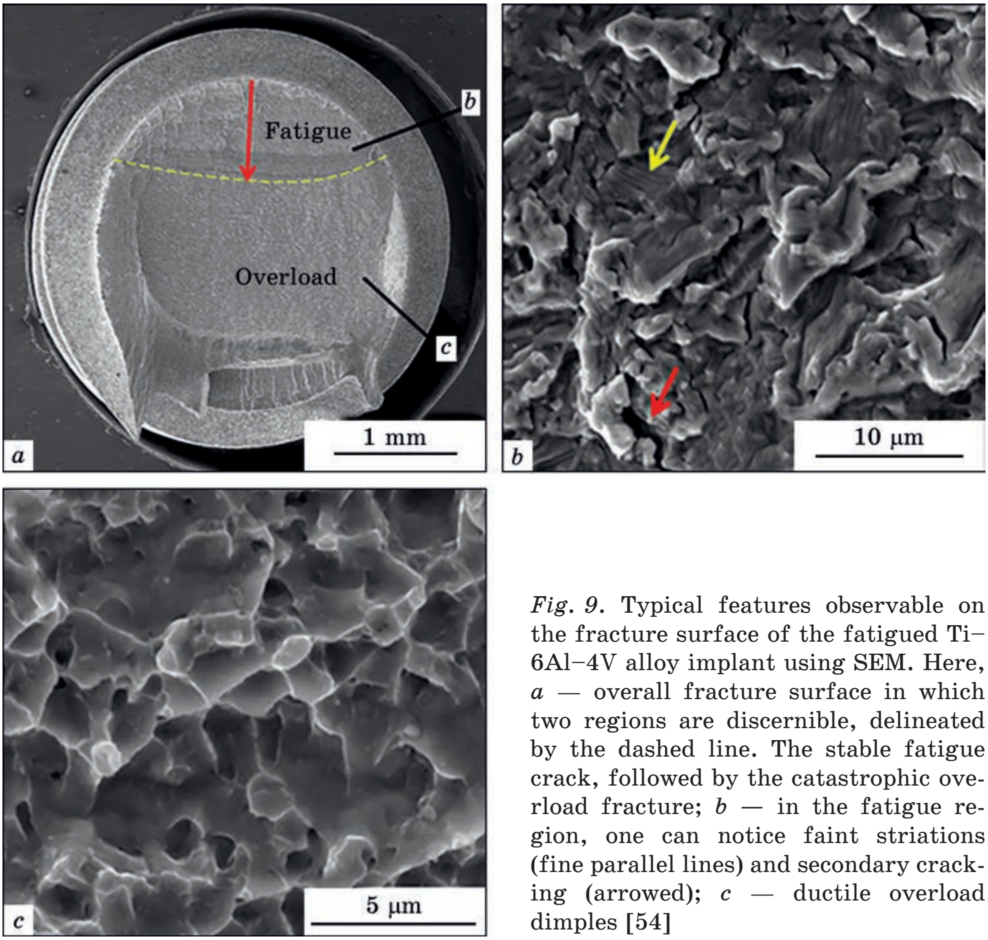

Fig. 9. Typical features observable on the fracture surface of the fatigued Ti–6Al–4V alloy implant using SEM. Here, *a* — overall fracture surface in which two regions are discernible, delineated by the dashed line. The stable fatigue crack, followed by the catastrophic overload fracture; *b* — in the fatigue region, one can notice faint striations (fine parallel lines) and secondary cracking (arrowed); *c* — ductile overload dimples [54]

the relatively high magnifications (Fig. 9, *b*). As for c.p.-Ti, the striations are usually quite apparent, but for the Ti–6Al–4V alloy, it may be more difficult to detect this feature. However, in such an alloy, one can see arrays of parallel microcracks that are perpendicular to the main fracture plane at the higher magnifications. The secondary cracks (Fig. 9, *b*) in the alloy are a clear indication of the fatigue failure process. As shown in Fig. 9, *c*, finally, when the fatigue crack becomes unstable, overload fracture ensues, which is characterised by microvoids (dimples). Therefore, one can conclude that the identification of fatigue as the fracture mechanism is well defined nowadays and is no longer subject to interpretations or guesswork.

The effect of the dental-implant diameter on the fatigue behaviour of the titanium alloy (Ti–6Al–4V) was studied with macro-failure analysis by SEM in Ref. [55]. To perform this experiment, conical 13-mm dental implants made of the titanium alloy were connected to a standard straight

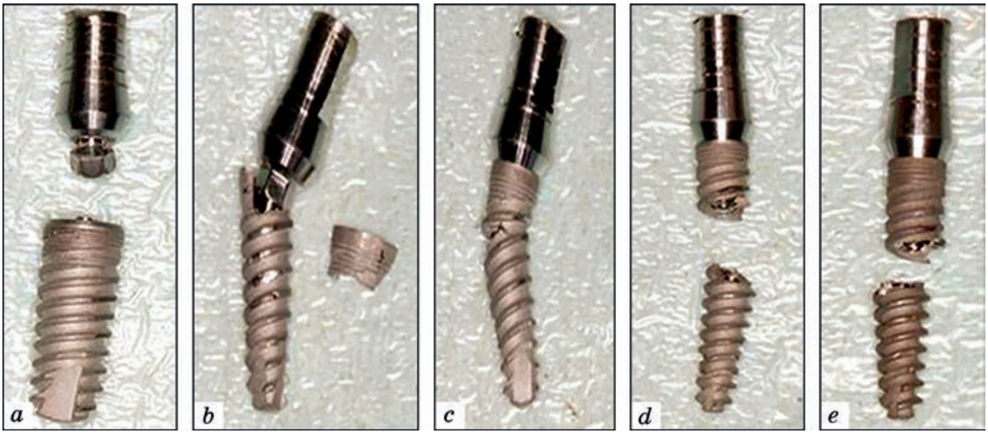

Fig. 10. The four modes of fracture: (*a*) 5-mm specimen broken on the screw and abutment neck; (*b*) 3.75-mm specimen broken on the implant neck; (*c*) 3.75-mm specimen broken on the implant second thread; (*d*) 3.3-mm specimen broken on the implant second thread; (*e*) 3.3-mm specimen broken on the implant third thread [55]

8-mm abutment using a 7-mm long screw. The implants of three diameters were tested for their fatigue performance: 3.3, 3.75, and 5 mm at the implant neck. The fatigue testing was performed under selected load control loads, which were applied as a sinusoidal regime to the implant abutment at an angle of 30° off-axis, inducing the bending moment. The test technique stopped operating when the implant fractured or when it reached $5\cdot10^6$ cycles without apparent failure. Eighty implants were fractured and analysed. The next four marked fracture types are identified in Fig. 10: the abutment neck and screw; the implant body–neck (the specimen was broken at the implant neck); implant body–thread 2 (the specimen was broken at the implant second thread); implant body-thread 3 (the specimen was broken at the implant third thread). It was observed that for the 5-mm implant, 100% of the fractured implants were fractured at the abutment neck and screw; for the 3.75-mm implant, 55.5% were fractured at the implants second thread, which is the dominant fracture mode, and 44.4% of the fractured implants were fractured at the neck of the implant; for the 3.3-mm implant, 52% of the fractured implants were fractured at the implants second tread and 48% were fracture at the implants third thread.

SEM representative macro- and microimages are presented in Fig. 11. There are two different regions of the macroscopic appearance of the failed implants. At the magnification between ×1000 and ×5000, the arrays of parallel secondary cracks are observed. These are parallel to the macroscopic crack front propagation direction. However, it is only at the relatively high magnifications (between 10 and 20 k) that one can discern faint striations, whose observation is not straightforward.

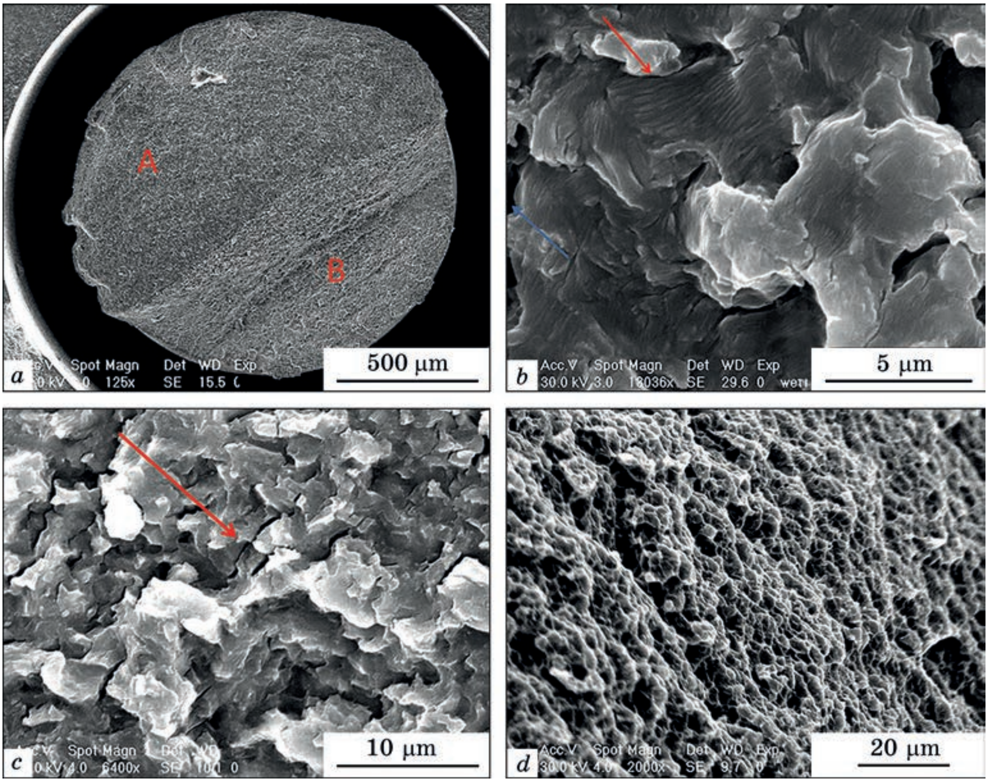

Fig. 11. (*a*) Fracture surface of the 5-mm implant. The maximum load was 852 N, and the specimen failed after 162,458 cycles. (*b*) The fatigue striation (see the arrow) between transgranular fractures indicating fatigue fracture for the 3.75-mm implant, with a maximum load of 810 N and 73,983 cycles to failure. (*c*) A view of the fatigue fracture mode found in the 3.3-mm implant. The maximum load was of 438 N, and the specimen failed after 1420000 cycles. (*d*) A view of the final fracture (monotonic overload) found on the fracture surface shown in the figure upper-left (*a*) [55]

There are different fracture modes of the 5-mm implant (Fig. 11, *a*), *i.e.*, *A* is a fatigue fracture, and *B* is the final fracture (monotonic overload). In the 3.3-mm implant (Fig. 11, *b*), fatigue failure does not originate from well-defined flaws and seems to have multiple sources. Fatigue failure is characterised by transgranular fracture with many secondary parallel cracks (arrow in Fig. 11, *c*) perpendicular to the local crack-front propagation. Note that fatigue striations are only discernible at relatively large magnifications, about ×10000. The final fracture failure is characterised by equiaxed dimples (Fig. 11, *d*) [55].

The main result of this study is as follows. Four distinctive fracture loci were identified, and macrofracture mode analysis was performed, showing that all 5-mm implants that fractured were fractured at the abutment neck and screw. In the 3.75-mm group, 44.4% were fractured at the

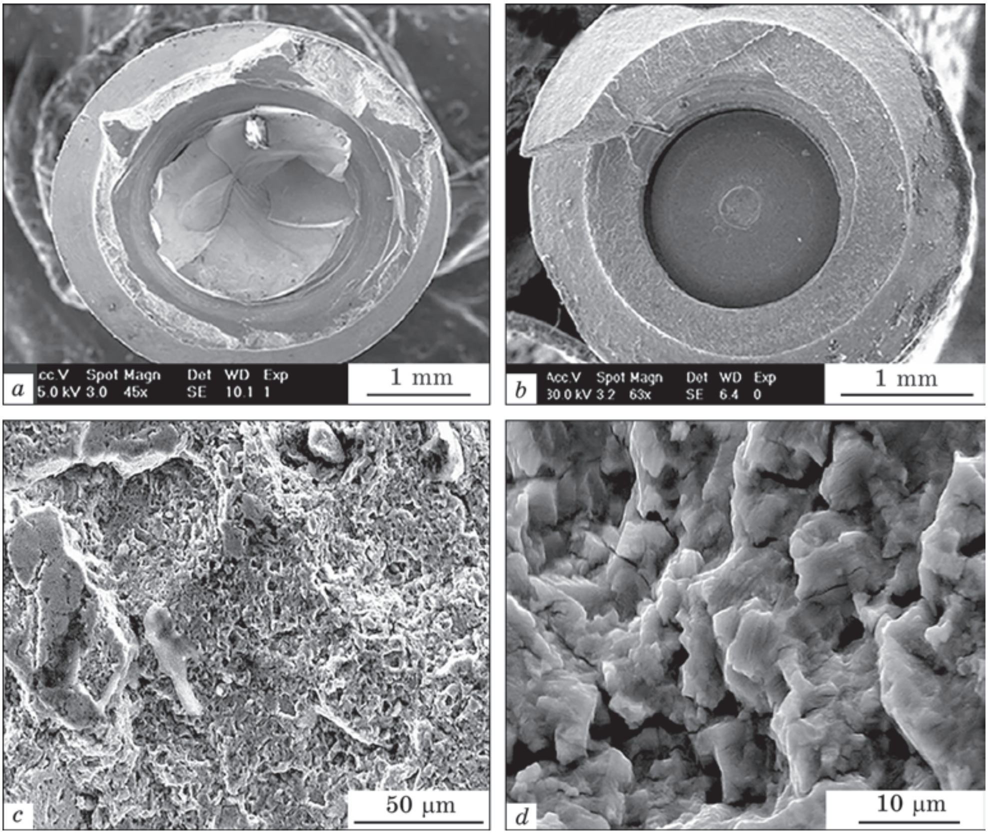

Fig. 12. Macrographic images of retrieved dental implants made of (*a*) c.p. Ti and (*b*) Ti–6Al–4V. (*c*) Final fracture in c.p. Ti dental implants: dimples from retrieved implant. (*d*) Fracture surface topography of Ti–6Al–4V dental implants: fractography taken from retrieved implants. Adopted from Ref. [56]

implant neck and 55.5% at the implants' second thread. Fifty-two per cent of the 3.3-mm fractured implants had it at the implants' second thread and 48% at the implant's third thread. The implants' metallographic sections revealed that the different fracture loci were located where thin metal cross sections and sharp notches coexist. Using SEM, it was able to characterise the failure micromechanisms and fatigue characterisation as transgranular fracture and arrays of secondary parallel microcracks at relatively low magnifications and classic fatigue striations at much higher magnifications.

The aim of the study [56] was to perform a detailed systematic failure analysis on Ti–6Al–4V alloy and c.p. Ti retrieved dental implants using the fractographic analysis in laboratory conditions. Figure 12 shows the representative macroscopic images of the retrieved dental implants' parts made of both c.p. Ti (*a*) and Ti–6Al–4V alloy (*b*). As seen, at the low mag-

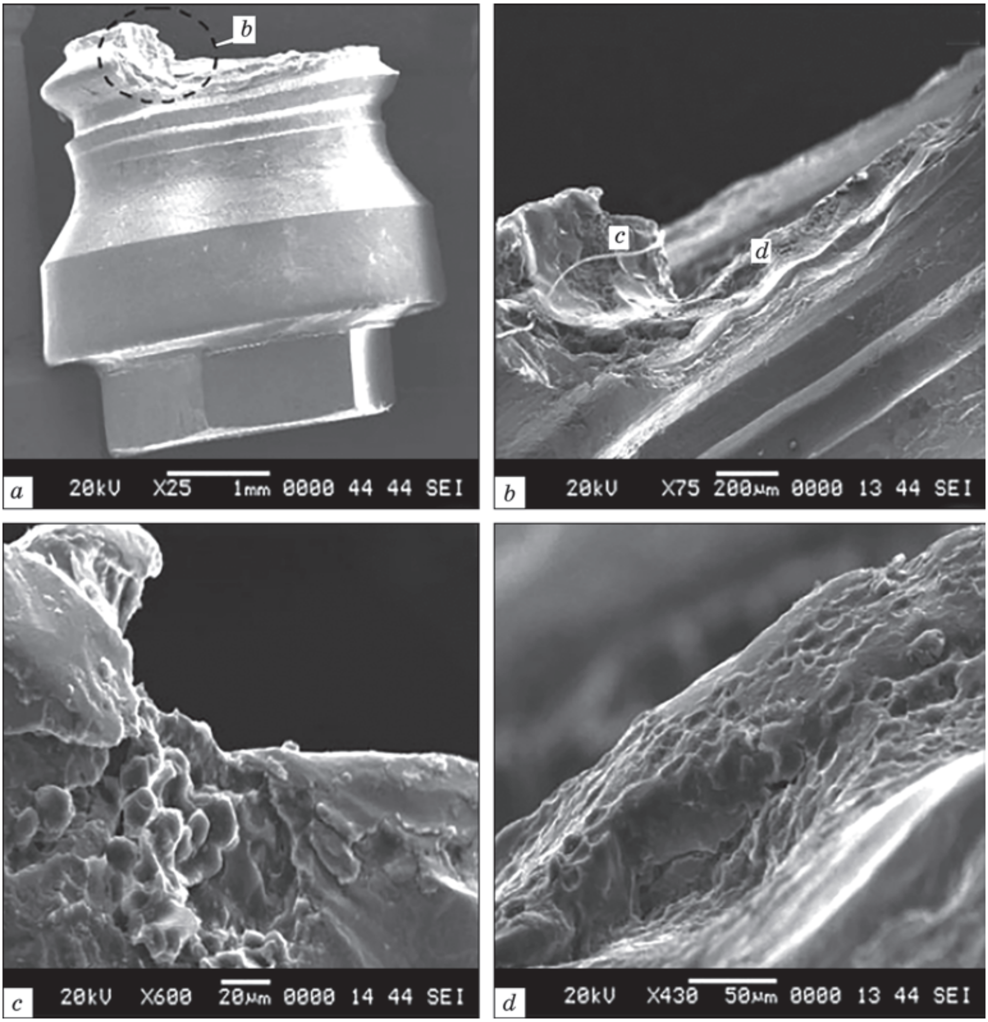

Fig. 13. SEM images of the retrieved upper part of the failed implant: (*a*) side view of the part with the damaged area enclosed in a circle; (*b*) magnification of the marked area in *a*; (*c*, *d*) indicate the areas magnified in *c* and *d*, respectively [57]

nification, the fracture surfaces are generally uniform and flat. This fact suggests the operation of a single failure mechanism until the final failure of the implant. Figures 12, *c, d* show the representative fracture surface topographies of the retrieved dental implants made of both c.p. Ti (*c*) and Ti–6Al–4V alloy (*d*). SEM images clearly reveal that fatigue is the dominant failure mechanism of the retrieved dental implants.

In the study [57], the commercially pure titanium implant-screw system failed after 15 years. The side view of the retrieved failed upper part of the implant is shown in Fig. 13, *a*. It is demonstrated that a fracture

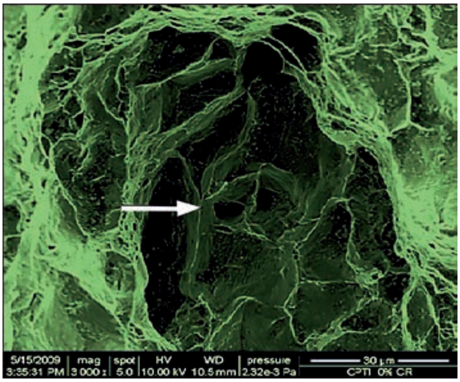

Fig. 14. SEM image with the intergranular fracture of the implant [58]

took place along the direction of the implant external thread, resulting in a step on the fracture surface. Interestingly, the implant surface at both sides of this step (Fig. 13, *b*) was covered by the characteristic globule formation (Fig. 13, *c*) and areas of cellular morphology (Fig. 13, *d*).

The system was retrieved in three pieces: the upper part of the implant, part of the abutment screw, and the apical part of the implant to which the screw part was installed. SEM observations carried out on all three retrieved parts demonstrated the synergistic effect of the distinct failure mechanisms, which led to total failure under extrinsic common fatigue loading. The microscopic observations failed because of the complex synergism of mechanisms. In the present study, total failure of both the dental implant and the abutment screw has been observed after 15 years of continuous function in the oral cavity of the patient. In the present case, the fractographic analysis revealed several peculiarities that support the activation of complementary mechanisms aggravating the common fatigue loading of the system.

In the present case [58], the titanium fractured implant segment was successfully removed and rehabilitated immediately with a larger diameter implant. It was found that the retrieved fracture segment had a diameter of 3.3 mm, and SEM analysis shows fatigue fractures, which may be the result of excessive overloading and use of the small-diameter implant, which enhances fatigue failure. An example of the fractured implant surface SEM image is shown in Fig. 14. Although the fractured surface is rather complex, the surface demonstrates evidence of intergranular fracture.

The (c.p. Ti) narrow dental implants (NDIs) fractured after being inserted in patients were observed in Ref. [59], and the fracture mechanism was fatigue in all cases. SEM fractography is shown in Fig. 15 with the detailed description of both crack nucleation points and the crack propagation paths. There are many longitudinal cracks along practically all vertices between the walls of the inner hexagonal connection. The crack nucleation is generated within the implant body, specifically in the inner hexagonal connection walls, just in the bottom horizontal ground plane. After crack nucleation, the progressive crack growth produced under cyclic masticatory multiaxial loading seems to describe the propagation path along the vertices of the hexagonal connection as well as through the wall thickness, as can be seen in Fig. 15, *b*. Different premature fatigue frac-

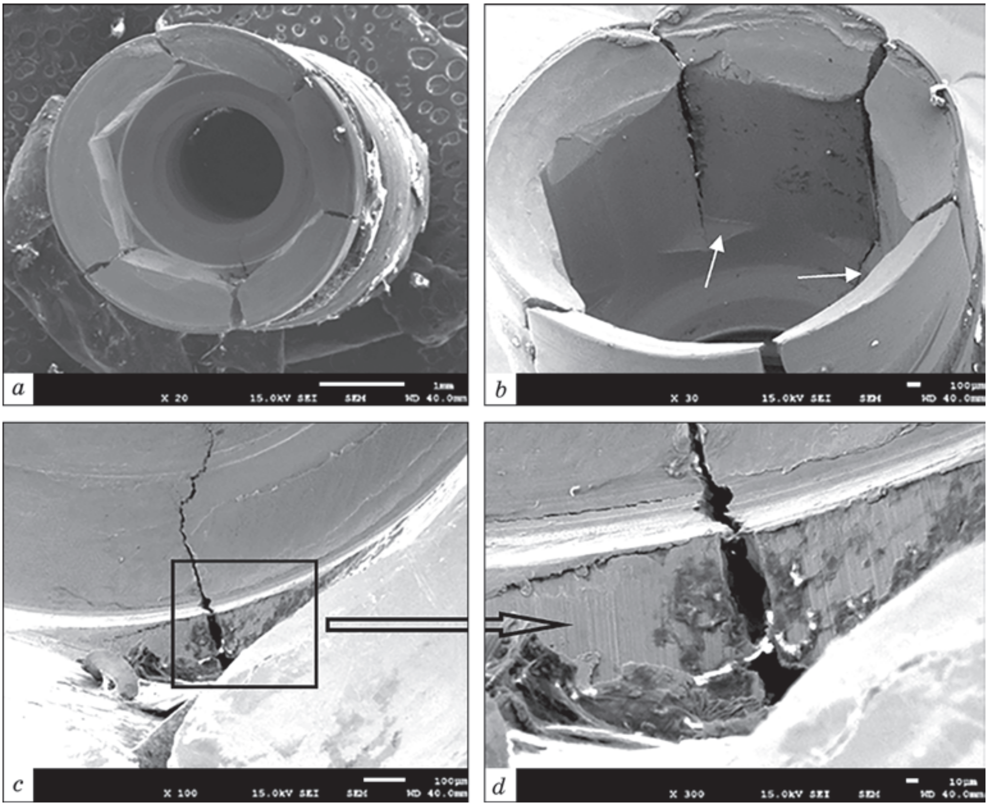

Fig. 15. SEM fractography of the explanted NDIs c.p. Ti implant: *a* — the explanted implant top view (×20); *b* — the micrograph of the hexagonal inner connection (side view) with detail of longitudinal fracture cracks (×30); *c* and *d* — the micrographs with the crack propagation detail at the different magnifications (×100 and ×300, respectively) [59]

tures have been observed due to the low mechanical properties and the defects in the surfaces produced in the conformation process.

The experiment [60] was conducted after the explanation of the clinical case, when the titanium Ti–6Al–4V alloy implant was fractured after successful osseointegration without any significant trauma or external force. The implant fixture dimension of 5.4 mm in diameter and 9 mm in height was placed in the native bone tissue. The antagonist was natural dentition with adequate occlusion. The crown had been in function for six years since its placement, and the fracture became noticeable due to its exaggerated movement. To evaluate the failed implant, the SEM was used at ×40, ×100, and ×500 magnifications (Fig. 16). The SEM visual analysis was performed to identify the fracture origin and crack pattern. The combination of the different factors, including abutment design misfit, material fatigue, and biomechanical stress imposed on the implant during func-

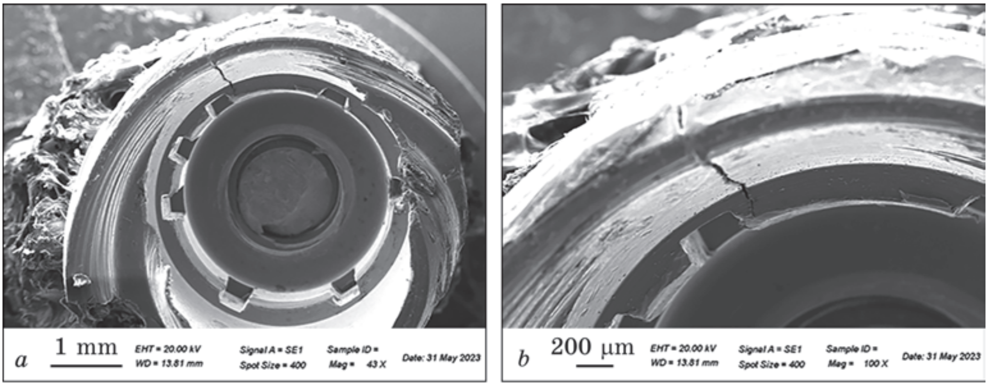

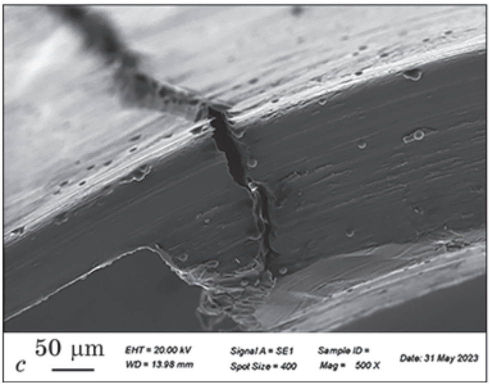

Fig. 16. SEM of the fractured retrieved dental implant showing: *a* — longitudinal crack originated from prosthetic platform at cervical level, descending to the implant apex (×40); *b* — magnification ×100, and magnification ×500 [60]

tional loading, was analysed. Fractures and mechanical failures not only require additional treatment interventions but also result in implant removal and replacement, leading to increased treatment costs, extended treatment duration, and patient dissatisfaction. Therefore, understanding the causes, risk factors, and preventive strategies for implant fractures and mechanical failures is crucial for ensuring long-term implant success. Further reports should be performed to elucidate the major causes as well as the risk factors associated with titanium fracture mechanics.

7. Contributing Factors for Fatigue Failure of Titanium Dental Implants (Gathered by Artificial Intelligence ChatGPT) [61]

Titanium dental implants demonstrate high long-term success rates; however, mechanical complications such as fatigue fracture remain a clinically significant cause of late implant failure. Fatigue failure results from the accumulation of microscopic damage under cyclic loading, even when applied stresses are below the ultimate tensile strength of the material. This section summarises the mechanisms of fatigue fracture in titanium dental implants reported in the current literature [61], focusing on loading conditions, material properties, implant design, biological factors, and the oral environment.

Titanium and its alloys, particularly commercially pure titanium (c.p. Ti) and Ti–6Al–4V, are widely used in dental implantology due to their favourable mechanical properties, corrosion resistance, and biocompatibility. Despite their high clinical success rates, implant fractures still occur, typically several years after functional loading. These failures are most often associated with metal fatigue, rather than overload or material defects alone. Fatigue-related implant fractures are considered late mechanical failures and are often irreversible, requiring implant removal. This section collects the principal factors contributing to fatigue failure of titanium dental implants.

Under cyclic loading in the oral environment, dental implants are exposed to complex and repetitive masticatory forces, which comprise: (i) axial forces during normal chewing, (ii) lateral and oblique forces during parafunctional activities, and (iii) high-frequency loading (up to several million cycles per year). Non-axial loading generates bending moments, which are particularly detrimental to implant fatigue resistance. Patients with bruxism exhibit significantly increased fatigue risk due to higher load magnitudes and cycle frequencies.

Fatigue cracks commonly initiate at areas of stress concentration, including the following: (i) implant threads, (ii) the implant neck region, (iii) the implant–abutment connection, (iv) microgaps and sharp geometric transitions. Small-diameter implants are especially susceptible to fatigue fracture due to reduced cross-sectional area and higher stress levels. Design features such as thread geometry, connection type (internal *vs*. external), and surface roughness play a crucial role in fatigue performance.

Material properties and microstructural factors are important for the implants' durability. Most modern dental implants are manufactured from Ti–6Al–4V alloy, which exhibits higher strength than c.p. Ti but may have lower fracture toughness under certain conditions. Fatigue resistance is influenced by the following: (i) grain size and crystallographic texture, (ii) presence of internal defects (pores, inclusions), and (iii) residual stresses induced during machining or surface treatment. Surface treatments (*e.g.*, sandblasting, acid etching) improve osseointegration but may also introduce micro-notches that act as fatigue crack-initiation sites.

The oral cavity represents an aggressive environment characterised by: (i) saliva with electrolytes, (ii) fluctuating pH values, (iii) temperature changes, and (iv) mechanical micromovements. These factors may disrupt the protective titanium oxide layer, leading to corrosion–fatigue synergy, where corrosion accelerates crack initiation and propagation under cyclic loading.

The synergetic influence of cycling and aggressive environment is supplemented by biological, clinical and prosthetic factors, which are the following: marginal bone resorption significantly increases fatigue risk by reducing the effective support length of the implant and by increasing bending stresses at the implant neck. Peri-implantitis is frequently associated with implant fractures, as progressive bone loss shifts stress concentration coronally. Thus, fatigue failure often reflects a combined mechanical–biological complication rather than a purely material problem. Several clinical factors which contribute to fatigue failure are the following: (i) improper occlusal design, (ii) excessive crown height space, (iii) misalignment between implant and prosthetic crown, and (iv) rigid prosthetic restorations without stress distribution. Prosthetic misfit can induce additional cyclic stresses at the implant–abutment interface, promoting fatigue crack initiation.

Preventing fatigue fracture requires a multidisciplinary approach, which can comprise the following actions: (i) adequate implant diameter and length selection, (ii) proper surgical positioning, (iii) optimisation of occlusion and prosthetic design, (iv) early detection and management of peri-implant bone loss, and (v) use of night guards in bruxism patients.

8. Conclusions

This paper studies the microstructural mechanism of fatigue failure of the titanium dental implants made of the technically pure titanium (c.p. Ti) and the Ti–6Al–4V alloy. The scanning electron microscopy observations of the fracture surfaces of two types of failed implant samples (*i.e.*, the implants taken from the patient after their failure and those tested in laboratory conditions under the action of cyclic loading in accordance with the European normative used for the mechanical tests (UNI EN ISO 14801)) were analysed.

As observed, the failure origin, loading history, environmental effects and surface material quality of the implant body and abutment can be elucidated using SEM of the fracture surfaces. As shown, fatigue is the main implant failure mechanism, and fatigue crack growth occurs through a three-stage pathway well known for metals, *i.e.*, stable crack propagation followed by accelerated crack propagation with apparent striations, and a final fast failure by void nucleation, coalescence and growth. At the same time, stress concentration on the implants' constructive peculiarities and corrosion damage, which can be induced by the aggressive oral environment, increases the probability of fatigue failure. Thus, without accounting for the biological, clinical and prosthetic factors, which are out of the scope of this paper, the surface modification methods, such as severe plastic deformation (shot peening, sand blasting, *etc*.), oxidation or coating, may help prevent the implant surface from damage and, thus, enhance the dental implant fatigue life.

Acknowledgements. The paper contains results carried out within the framework of the project (state reg. No. 0124U001001) of the Ministry of Education and Science of Ukraine.

Authors' Contributions. B.M.M. collected the literature data regarding the applicability of titanium dental implants, analysed the operative factors and fatigue mechanism, as well as performed review and editing of the manuscript. M.O.V. designed the review concept, collected and analysed the literature data regarding mechanical complications and titanium implant testing and failures, communicated with ChatGPT, and prepared the first draft of the manuscript. S.M.V. collected and analysed the literature data regarding laboratory fatigue tests of dental implants and various fracture modes. P.O.H reviewed and analysed the literature regarding fatigue of the retrieved failed implants. All authors approved the final version of the manuscript.

REFERENCES

1. R.M. Sullivan, *J. Calif. Dent. Assoc.*, **745**, No. 11: 737 (2001); https://pubmed.ncbi.nlm.nih.gov/11806052
2. J.H. Lee, V. Frias, K.W. Lee, and R.F. Wright, *J. Prosthet. Dent.*, **94**: 377 (2005); https://doi.org/10.1016/j.prosdent.2005.04.018
3. L. Gaviria, J.P. Salcido, T. Guda, and J.L. Ong, *J. Korean Assoc. Oral Maxillofac Surg.*, **40**: 50 (2014); https://doi.org/10.5125/jkaoms.2014.40.2.50
4. A. Delantoni, D. Nur Sengun, and K. Orhan, *Genel Tıp Derg.* **35**, No. 3: 512 (2025); https://doi.org/10.54005/geneltip.1643015
5. C.A. Babbush, J.A. Hahn, J.T. Krauser, and J.L. Rosenlicht, *Dental Implants: The Art and Science* (Elsevier Health Sciences: 2010).
6. L.O. Massa and J.A. von Fraunhofer, *The ADA Practical Guide to Dental Implants* (The American Dental Association: 2021).
7. M. Armentia, M. Abasolo, I. Coria, and J. Albizuri, *Metals*, **10**: 744 (2020); https://doi.org/10.3390/met10060744
8. B. Ziaie and S.M. Reza Khalili, *Prosthesis*, **3**: 300 (2021); https://doi.org/10.3390/prosthesis3040028
9. S. Fuda, B.G.D.S. Martins, F.C.D. Castro, A. Heboyan, S.A. Gehrke, J.C.H. Fernandes, A.C.V. Mello-Moura, and G.V.O. Fernandes, *Diagnostics*, **13**: 1587 (2023); https://doi.org/10.3390/diagnostics13091587
10. G.E. Romanos, *Implant Dent.*, **28**, No. 6: 522 (2019); https://doi.org/10.1097/ID.0000000000000940
11. A. Verma, S.V. Singh, D. Arya, S. Shivakumar, and P. Chand, *J. Oral Biology Craniofacial Res.*, **13**: 306 (2023); https://doi.org/10.1016/j.jobcr.2023.02.009
12. A.S. el Askary, R.M. Meffert, and T. Griffin, *Implant Dent.*, **8**, No. 2: 173 (1999); https://pubmed.ncbi.nlm.nih.gov/10635160
13. P. Atalay, *J. Dental. Sci.*, **7**, No. 4: 000349 (2022); https://doi.org/10.23880/oajds-16000349

14. T.A. Do, H.S. Le, Y.W. Shen, H.L. Huang, and L.J. Fuh, *Int. J. Environ. Res. Public Health*, **17**: 3931 (2020);
https://doi.org/10.3390/ijerph17113931
15. G.R.S. Lopes, J.D.M. Matos, D.A. Queiroz, J.P.M. Tribst, N.C. Ramos, M.G. Rocha, and A.B. Barbos, *Materials,* **15**: 6235 (2022);
https://doi.org/10.3390/ma15186235
16. H.M. Huang, C.M. Tsai, C.C. Chang, C.T. Lin, and S.Y. Lee, *Int. J. Oral Maxillofacial Implants*, **20**, No. 6: 854 (2005);
https://pubmed.ncbi.nlm.nih.gov/16392341
17. Archana Singh, Ankita Singh, R. Vivek, T.P. Chaturvedi, P. Chauhan, and S. Gupta, *Case Reports in Dentistry*, **2013**: 270385 (2013);
https://doi.org/10.1155/2013/270385
18. G.A. Zarb and A. Schmitt, *J. Prosthet. Dent.*, **64**: 185 (1990);
https://doi.org/10.1016/0022-3913(90)90177-E
19. M.R. Norton, *Clin. Oral Implants Res.*, **8**: 290 (1997);
https://doi.org/10.1034/j.1600-0501.1997.080407.x
20. A. Sánchez-Pérez, M. José Moya-Villaescusa, A. Jornet-García, and S. Gomez, *Med. Oral Patol. Oral Cir. Bucal.*, **15**, No. 3: e504 (2010);
https://doi.org/10.4317/medoral.15.e504
21. T.J. Balshi, *Int. J. Oral Maxillofacial Implants*, **11**: 660 (1996);
https://pubmed.ncbi.nlm.nih.gov/8908866
22. N.T. Green, E.E. Machtei, J. Horwitz, and M. Peled, *Implant Dent.*, **11**: 137 (2002).
https://doi.org/10.1097/00008505-200204000-00014
23. P. Virdee and K. Bishop, *Br. Dent. J.*, **203**: 461 (2007);
https://doi.org/10.1038/bdj.2007.948
24. S. Sanivarapu, S. Moogla, R. Kuntcham, and L. Kolaparthy, *J. Indian Soc. Periodontol.*, **20**: 6 (2016);
https://doi.org/10.4103/0972-124X.154190
25. A. Shibli, E. Marcantonio, S. d'Avila, A.C. Guastaldi, and E. Marcantonio, *J. Periodontol.*, **76**, No. 7: 1092 (2005);
https://doi.org/10.1902/jop.2005.76.7.1092
26. F.J. Gil, E. Espinar, J.M. Llamas, and P. Sevilla, *Clinical Implant Dentistry and Related Research*, **16**, No. 2: 273 (2014);
https://doi.org/10.1111/j.1708-8208.2012.00468.x
27. C. Fleck and D. Eifler, *Int. J. Fatigue*, **32**: 929 (2010);
https://doi.org/10.1016/j.ijfatigue.2009.09.009
28. P.I. Bånemark, B.O. Hansson, R. Adell, U. Breine, J. Lindström, O. Hallén, and A. Ohman, *Scand. J. Plast. Reconstruct. Surg. Suppl.*, **16**: 1 (1977);
https://pubmed.ncbi.nlm.nih.gov/356184
29. P.I. Brånemark, R. Adell, T. Albrektsson, U. Lekholm, S. Lundkvist, and B. Rockier, *Biomater.*, **4**: 25 (1983);
https://doi.org/10.1016/0142-9612(83)90065-0
30. J.R. Davis, *Handbook of Materials for Medical Devices* (ASM International: 2003).
31. E.A.B. Effah, P.D. Bianco, and P. Ducheyne, *J. Biomed. Mater. Res.*, **73**: 80 (1995);
https://doi.org/10.1002/jbm.820290111
32. J.E. Ellingsen, *Biomater.*, **12**: 593 (1991);
https://doi.org/10.1016/0142-9612(91)90057-H
33. T. Hanawa, K. Asami, and K. Asaoka, *J. Biomed. Mater. Res.*, **40**: 530 (1998);
https://doi.org/10.1002/(SICI)1097-4636(19980615)40:4%3C530::AID-JBM3%3E3.0.CO;2-G

34. M. Geetha, A.K. Singh, R. Asokamani, and A.K. Gogia, *Prog. Mater. Sci.*, **54**, No. 3: 397 (2009);
https://doi.org/10.1016/j.pmatsci.2008.06.004
35. I.S. Park, S.Y. Won, T.S. Bae, K.Y. Song, C.W. Park, T.G. Eom, and C.M. Jeong, *Met. Mater. Int.*, **14**, No. 2: 133 (2008);
ttps://doi.org/10.3365/met.mat.2008.04.133
36. C.K. Lee, *Evaluation of Test Protocol Variables for Dental Implant Fatigue Research* (SoDM Masters Theses, 149) (2007);
https://opencommons.uconn.edu/sodm_masters/149
37. E. Marchetti, S. Ratta, S. Mummolo, S. Tecco, R. Pecci, R. Bedini, and G. Marzo, *Implant Dent.*, **25**, No. 5: 613 (2016);
https://doi.org/10.1097/ID.0000000000000453
38. M.A.L. Hernandez-Rodriguez, G.R. Contreras-Hernandez, A. Juarez-Hernandez, B. Beltran-Ramirez, and E. Garcia-Sanchez, *Eng. Failure Anal.*, **57**: 236242 (2015);
https://doi.org/10.1016/j.engfailanal.2015.07.035
39. E. Marchetti, S. Ratta, S. Mummolo, S. Tecco, R. Pecci, R. Bedini, and G. Marzo, *Implant Dent.*, **25**, No. 5: 613 (2016);
https://doi.org/10.1097/ID.0000000000000453
40. ISO 14801:2016. *Dentistry-Implants-Dynamic Loading Test for Endosseous Dental Implants* (Geneva: Int. Org. for Standardization: 2016);
https://www.iso.org/standard/61997.html
41. G.H. Do, S.J. Lee, J.M. Kim, and S.M. Kim, *J. Appl. Reliability*, **17**, No. 1: 50 (2017);
https://koreascience.kr/article/JAKO201722647667302.pub
42. C.K. Lee, M. Karl, and J.R. Kelly, *Dent. Mater.*, **25**: 1419 (2002);
https://doi.org/10.1016/j.dental.2009.07.003
43. L. Lawson, E.Y. Chen, and M. Meshii, *Int. J. Fatigue*, **21**: S15–S34 (1999);
https://doi.org/10.1016/S0142-1123(99)00053-5
44. H. Mughrabi, H.W. Hцppel, and M. Kautz, *Scripta Mater.*, **51**: 807 (2004);
https://doi.org/10.1016/j.scriptamat.2004.05.012
45. N. Maruyama, Mechanical testing of metallic biomaterials, *Metals for Biomedical Devices* (Ed. M. Niinomi) (Woodhead Publishing–CRC Press: 2010), Ch. 6, p. 157–177;
https://doi.org/10.1533/9781845699246.2.157
46. S.M. Voloshko, B.M. Mordyuk, M.O. Vasylyev, and A.P. Burmak, Microstructure and fatigue behaviour of AlSi10Mg alloy samples fabricated by selective laser melting, *Prog. Phys. Met.*, **27**, No. 1: 130 (2026);
https://doi.org/10.15407/ufm.27.01.130
47. B.N. Mordyuk and G.I. Prokopenko, *Mater. Sci. Eng. A*, **437**: 396 (2006);
https://doi.org/10.1016/j.msea.2006.07.119
48. B.N. Mordyuk, A.I. Dekhtyar, D.G. Savvakin, and N.I. Khripta, *J. Mater. Eng. Perform.*, **31**: 5668 (2022);
https://doi.org/10.1007/s11665-022-06633-7
49. F.A. Shah, M. Trobos, P. Thomsen, and A. Palmquist, *Mater. Sci. Eng. C*, **62**: 960 (2016);
https://doi.org/10.1016/j.msec.2016. 01.032
50. A.I. Dekhtyar, B.N. Mordyuk, D.G. Savvakin, V.I. Bondarchuk, I.V. Moiseeva, and N.I. Khripta, *Mater. Sci. Eng. A*, **641**: 348 (2015);
https://doi.org/10.1016/j.msea.2015.06.072
51. B.N. Mordyuk, G.I. Prokopenko, Yu.V. Milman, M.O. Iefimov, and A.V. Sameljuk, *Mater. Sci. Eng. A*, **563**: 138 (2013);
https://doi.org/10.1016/j.msea.2012.11.061

52. H.G. Fan, X.Q. Gan, and Z.O. Zhu, *Int. J. Clin. Exp. Med.*, **10**, No. 4: 6369 (2017); www.ijcem.com /ISSN:1940-5901/IJCEM0045638
53. S.A. Hoyer, C.M. Stanford, S. Buranadham, T. Fridrich, J. Wagner, and D. Gratton, *J. Prosthet. Dent.*, **85**: 59 (2001); https://doi.org/10.1067/mpr.2001.115250
54. K. Shemtov-Yona and D. Rittel, *Dent. J.*, **4**, No. 2: 16 (2016); https://doi.org/10.3390/dj4020016
55. K. Shemtov-Yona, D. Rittel, E.E. Machtei, and L. Levin, *Clinical Implant Dent. Related Res.*, **16**, No. 2: 178 (2012); https://doi.org/10.1111/j.1708-8208.2012.00476.x
56. K. Shemtov-Yona and D. Rittel, *Eng. Failure Anal.*, **38**: 58 (2014); https://doi.org/10.1016/j.engfailanal.2014.01.002
57. M.G. Manda, P.P. Psyllaki, D.N. Tsipas, and P.T. Koidis, *J. Biomed. Mater. Res. Part B: Appl. Biomater.*, **89B**, No. 1: 264 (2009); https://doi.org/10.1002/jbm.b.31211
58. T. Berglundh, L. Persson, and B. Klinge, *J. Clinical Periodontology*, **29**, No. 3: 197 (2002); https://doi.org/10.1034/j.1600-051X.29.s3.12.x
59. E. Velasco, A. Flichy-Fernández, M. Punset, A. Jiménez-Guerra, J.M. Manero, and F.J. Gil, *Mater.*, **12**, No. 12: 3728 (2019); https://doi.org/10.3390/ma12223728
60. J.P.M. Tribst, A. Werner, and E.J. Blom, *Diagnostics*, **13**: 2123 (2023); https://doi.org/10.3390/diagnostics13122123
61. Chat GPT Artificial Intelligence, *Fatigue Failure of Titanium Dental Implants: Mechanisms, Contributing Factors, and Clinical Implications* (communication on 2026.01.05).

Received 27.02.2026
Final version 03.08.2026

М.О. Васильєв[1], *Б.М. Мордюк*[1], *С.М. Волошко*[2], *П.О. Гурин*[3]
[1] Інститут металофізики ім. Г.В. Курдюмова НАН України,
бульв. Академіка Вернадського, 36, 03142 Київ, Україна
[2] Національний технічний університет України
«Київський політехнічний інститут імені Ігоря Сікорського,
Берестейський просп., 37, 03056 Київ, Україна
[3] Національний університет охорони здоров'я України імені П.Л. Шупика,
вул. Дорогожицька, 9, 04112 Київ, Україна

АНАЛІЗ ПОВЕРХНІ ЗЛАМУ ТИТАНОВИХ ЗУБНИХ ІМПЛАНТАТІВ ПІСЛЯ ВТОМНОГО РУЙНУВАННЯ

Упродовж останніх десятиліть стоматологічна галузь зазнала революційних змін завдяки впровадженню титанових остеоінтегрованих зубних імплантатів, що дало змогу відновлювати функцію ротової порожнини. Такі імплантати вирізняються високою надійністю і демонструють чудові результати за тривалого використання. Однак механічні ускладнення, подібні до втомного руйнування, залишаються клінічно значущою причиною пізнього відторгнення імплантатів. Це — одне з важливих біомеханічних ускладнень, яке може становити значну проблему як для пацієнта, так і для стоматолога. Головною метою цієї роботи є з'ясування мікроструктурного механізму втомного руйнування титанових зубних імплантатів. Досліджено поверхні двох типів зразків імплантатів, що руйнуються, виготовлених з технічно (комерційно) чистого титану (c.p. Ti) та сплаву Ti–6Al–4V. Зразки першого типу було випробувано в лабораторних умовах під дією циклічного навантаження відповідно до європейського стандарту, що використовується для механічних випробувань (UNI EN ISO 14801); інші зразки імплантатів було вилучено у пацієнтів після руйнування. Використання сканувальної електронної мікроскопії (СЕМ) для дослідження поверхні зламу надало інформацію про походження руйнування, історію навантаження, вплив навколишнього середовища та якість матеріалу поверхні тіла імплантату і коронки. За допомогою СЕМ підтверджено, що втома є основним механізмом руйнування імплантату, який складається з тристадійного процесу, добре відомого стосовно металів, а саме: стабільне поширення тріщини з наступним її пришвидшеним поширенням і фінальним швидким руйнуванням шляхом формування, коалесценції та збільшення пор. Попри дотримання вимог щодо мікроструктури імплантату, концентрація напружень на його конструктивних особливостях і корозійних пошкодженнях, що може виникнути через агресивне середовище ротової порожнини, підвищує ризик його втомного руйнування.

Ключові слова: зубні імплантати, титан, сплав Ti–6Al–4V, втомне руйнування, циклічне навантаження, руйнування імплантату.